


RESEARCH

Open Access



# Flexural Behaviour of Reinforced Concrete Beams Strengthened with Textile-Reinforced Strain Hardening Geopolymer Composites (TR-SHGC)

Mohamed Wasef<sup>1</sup>, Ali Hassan<sup>1\*</sup>  and Nesreen M. Kassem<sup>1</sup>

## Abstract

This study aims to assess the behaviour of Reinforced Concrete (RC) beams strengthened in flexure with a composite layer of strain-hardening geopolymer composites (SHGC) and Fiber Reinforced Polymer (FRP) textiles. One unstrengthened reference beam and ten strengthened beams were tested under static loading conditions. The tested beams had similar dimensions: a total depth of 250 mm, a width of 200 mm, a total length of 2400 mm and a clear span of 2200 mm. The textile-reinforced mortar (TRM) strengthening was applied in the form of either externally bonded (EB) or hybrid near surface embedded and externally bonded (NSEEB) technique. Thus, before the strengthening applications, longitudinal grooves were created in the soffit of nine beams: in eight beams, a groove with a depth of 25 mm and a width of 100 mm was created, whereas, in one beam, two grooves with a depth of 25 mm and a width of 50 mm were made. This study compares three types of strengthening mortars: ordinary cementitious mortar (OM), strain-hardening cementitious composites (SHCC), and SHGC. Embedded into the mortar, either null, one, two or three layers of textile reinforcement were provided. The mortar reinforcement was either steel, GFRP or CFRP. The test results showed that the application of SHGC in the form of the NSEEB technique increased the ultimate load and ductility of the strengthened beams. With the strengthening of NSEEB-SHGC, the improvement in the ultimate capacity reached about 67%. Finally, a flexural capacity model was proposed that agreed with the experimental results.

**Keywords** Strengthening, Flexure, Concrete, Beams, Strain hardening cementitious composites (SHCC), Strain hardening geopolymer composites (SHGC)

## 1 Introduction

There are many existing systems for the strengthening of RC flexural members. In the last years, the Fiber Reinforced Polymers (FRP) has attracted many concerns (Imjai et al., 2022). The main advantages of the FRP are

ease of application, the high strength-to-weight ratio and high resistance to corrosion, (Dai et al., 2005; Imjai et al., 2023). Despite its advantages, the Externally Bonded (EB) FRP systems typically bonded with epoxy show poor fire resistance and limited compatibility with concrete in moist environments (Bisby et al., 2005). In addition, the debonding-controlled failure between the EB-FRP and the concrete substrates is a critical issue (Lu et al., 2005). The debonding often occurs at the cutoff or crack locations (intermediate crack debonding (IC)) (Imjai et al., 2016; Lu et al., 2005).

Journal information: ISSN 1976-0485/eISSN 2234-1315.

\*Correspondence:

Ali Hassan

ali\_hassan@f-eng.tanta.edu.eg

<sup>1</sup> Structural Engineering Department, Faculty of Engineering, Tanta University, Tanta 31511, Egypt



© The Author(s) 2025. **Open Access** This article is licensed under a Creative Commons Attribution 4.0 International License, which permits use, sharing, adaptation, distribution and reproduction in any medium or format, as long as you give appropriate credit to the original author(s) and the source, provide a link to the Creative Commons licence, and indicate if changes were made. The images or other third party material in this article are included in the article's Creative Commons licence, unless indicated otherwise in a credit line to the material. If material is not included in the article's Creative Commons licence and your intended use is not permitted by statutory regulation or exceeds the permitted use, you will need to obtain permission directly from the copyright holder. To view a copy of this licence, visit <http://creativecommons.org/licenses/by/4.0/>.

Fabric-reinforced cementitious matrix (FRCM) has been proposed to avoid the problems of EP-FRP strengthening. FRCM consists of FRP textile grids embedded into a cementitious matrix (bonding material). Polymer-modified cementitious mortar or ordinary cementitious mortar were used as cementitious bonding matrices in the FRCM system (Gonzalez-Libreros et al., 2017b). Several experimental investigations have been conducted to figure out the feasibility of the FRCM strengthening system for flexural/shear strengthening of RC beams (Aljzaeri et al., 2019; Elsanadedy et al., 2013; Gonzalez-Libreros et al., 2017a; Tetta et al., 2018; Wakjira & Ebead, 2019), slabs (Kadhim et al., 2022) and columns (Colajanni et al., 2014; Faleschini et al., 2020; Napoli & Realfonzo, 2020). As presented in previous work, the ultimate tensile strain of the FRP embedded into the FRCM is less than that bonded with the epoxy (Gonzalez-Libreros et al., 2017a). This is owing to the brittleness of the ordinary cementitious mortars. In addition, the failure of FRCM strengthening commonly takes place due to fabric slippage from the bonding matrix or debonding from the concrete substrate (Giese et al., 2021).

Strain Hardening Cementitious Composites (SHCC) belong to the high-performance fiber-reinforced cementitious composites (HPRCC). The strain capacity of SHCC under tensile loads ranges between 2 and 10% (Li, 1993; Li et al., 2001), in addition to, the advantages of high tensile strength, fracture energy and improved cracking behaviour (Hassan et al., 2022; Li, 2003; Liu et al., 2017). Elements strengthened with SHCC layers have excellent corrosion resistance owing to the invasion of the corrosive media with SHCC protection, which generally experiences a favorable multiple microcracking behaviour under tension (Sahmaran et al., 2015). Recently, the FRP grid-reinforced SHCC matrix has been proposed as an efficient strengthening system (Ye et al., 2021; Zheng et al., 2018). Instead of traditional mortars, SHCC could be employed as a bonding matrix to avoid the interface debonding between the strengthening mortar and concrete substrate (Pan et al., 2022). In addition, using the SHCC as the bonding matrix overcomes the low ductility of traditional cementitious mortars, accordingly, a full utilization of the FRP strength could be achieved (Pan et al., 2022). In addition, the FRP reinforcement improves both the strength capacity and failure toughness of the cementitious composites (Pan et al., 2022). To date, several research has been conducted to assess the feasibility of FRP-SHCC as a flexural strengthening composite system. The investigated parameters were the form of application (i.e., cast-in-place layer or precast plates), the thickness of the layer, the reinforcement in the layer (ratio and type), the reinforcement ratio of the strengthened member and the treatment method

of the concrete substrate (Pan et al., 2022). As reported in previous studies, good surface treatment played an important role in achieving effective strengthening (Yang et al., 2018). In addition, the use of SHCC at the tension zone increased the moment capacity owing to the tensile hardening of the SHCC (Wei et al., 2020). The numerous advantages of SHCC paved the practical application for strengthening/repairing many structures (Kunieda and Rokugo, 2006; Li, 1998). However, the cement-based composites (SHCC) exhibits high carbon emissions, owing to the high cement dosage in SHCC mixtures. Thus, strain-hardening geopolymer composites (SHGC) are developed that could be a good alternative to the cement-based SHCC (Duxson et al., 2007a, 2007b; Kong & Sanjayan, 2010; Li et al., 2004; Sagoe-Crentsil et al., 2013).

Like SHCC, SHGC can exhibit multiple fine cracks in conjunction with high strain capacity and ductility at ultimate load under tensile loads (Koutas & Papakonstantinou, 2021; Lee et al., 2012; Nematollahi et al., 2014, 2015; Peng et al., 2022; Shaikh, 2013; Shen et al., 2021). Moreover, the SHGC has acid and fire resistance higher than the SHCC (Kong & Sanjayan, 2010). Razak et al. (2021) and Al Saffar et al. (2020) investigated the behaviour of geopolymer composites under the influence of high temperatures and fire. The geopolymer composites showed very great capabilities to withstand high temperatures. The capability of geopolymer composites may reach 900, 1200 degrees Celsius (Al Saffar et al., 2020; Razak et al., 2021). This made the geopolymer composites on the platform of the construction of buildings that can be used in many applications that are subject to high temperatures or fires compared to ordinary cement-based mortar.

The effect of FRP-SHGC strengthening on the flexural behaviour of RC beams has not been studied widely and needs more investigation. Thus, the current study aims to evaluate the adequacy of a composite layer of the FRP-SHGC for improving the flexural behaviour of RC beams. The studied parameters were the bonding mortar, the strengthening technique (NSEEB or EB), the type of textile reinforcement and the number of textile layers. The test results in terms of failure mode, ultimate capacity, load-deflection response, load-strain response and the maximum crack width readings are presented and discussed. Besides, an analytical investigation was carried out to calculate the flexural capacity of the TR-SHGC strengthened beams.

## 2 Experimental Work Program

### 2.1 Description of the Test Program

Experimental tests were carried out on eleven RC beams; one unstrengthened beam and ten strengthened beams. Fig. 1 shows the shape, dimensions, reinforcement details

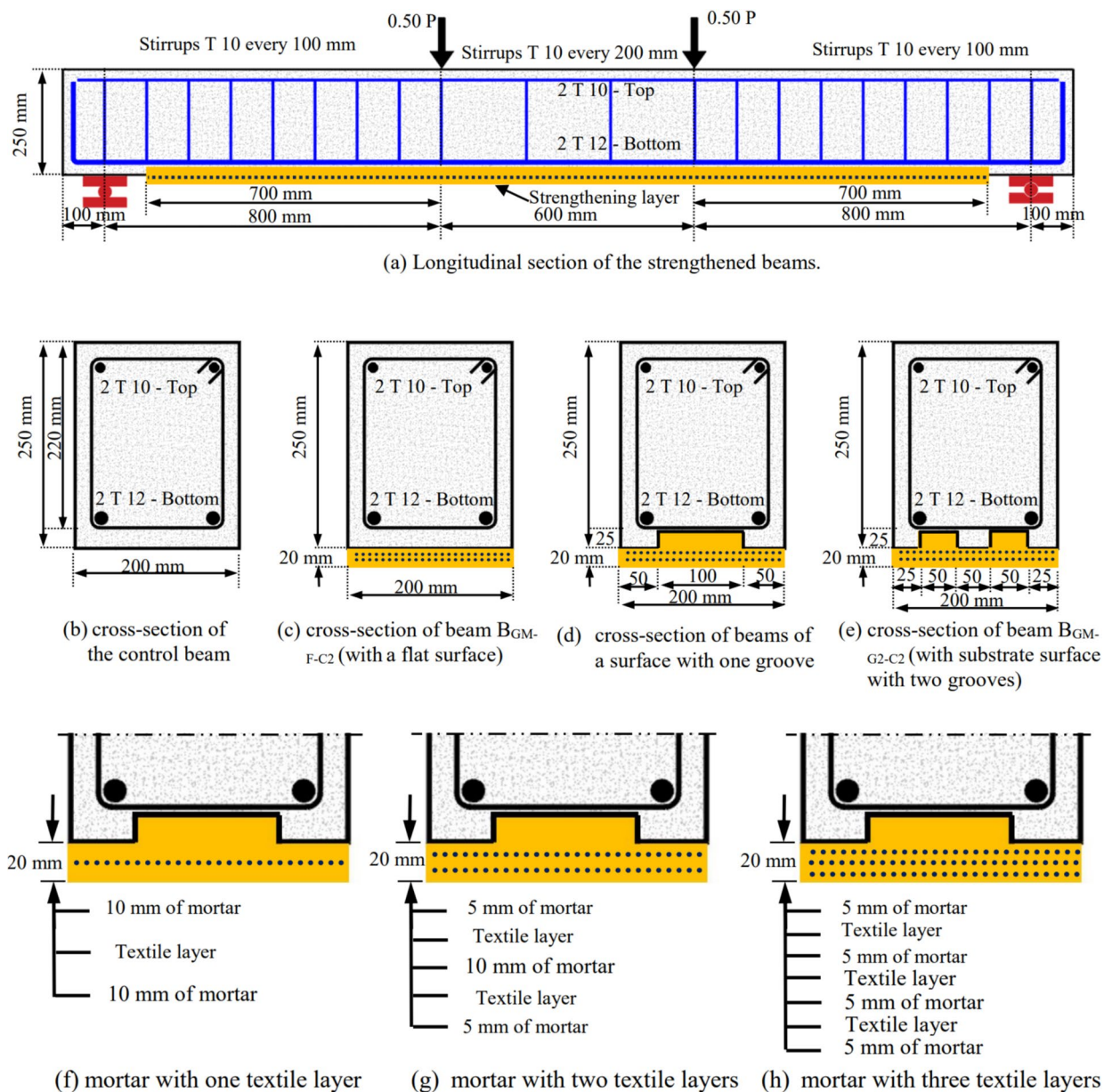


**Fig. 1** Details of the tested beams.

and strengthening details of the studied beams. All beams were similar in geometrical dimensions and internal steel reinforcement. The beams had a total length and an effective span of 2400 and 2200 mm, respectively. The beams had a width and a total depth of 200 and 250 mm, respectively. The concrete cover of the tension steel reinforcement was 30 mm. The longitudinal reinforcement of the beams consisted of 2 T 12 mm and 2 T 10 mm for the tension and compression reinforcement, respectively. The used tension reinforcement ratio (0.45%) ensures a tension-controlled failure mode according to the current

ACI 318 (2019). Each shear zone was provided with stirrups of 10 mm diameter spaced at 100 mm (center-to-center spacing). Whereas, at the constant moment zone, the spacing of stirrups was 200 mm.

Table 1 lists the parameters of the study. As shown in the table, the experimental program involved a control beam (unstrengthened) and ten strengthened beams. Fig. 1 shows the details of the used strengthening. As shown in Fig. 1, the strengthening was applied in the form of either the NSEEB or EB technique. The strengthening layer provides an additional thickness of 20 mm

**Table 1** Description of test specimens.

Group	Beam's designation	Bonding mortar	Surface condition	Mortar reinforcement		Studied parameter
				Type	No. of layers	
Control	BC	–	Flat	–	–	Reference
Group I	B <sub>OM-G1-C2</sub>	OM	With one groove	CFRP	Two	Type of mortar
	B <sub>CM-G1-C2</sub>	SHCC	With one groove	CFRP	Two	
	B <sub>GM-G1-C2</sub>	SHGC	With one groove	CFRP	Two	
Group II	B <sub>GM-F-C2</sub>	SHGC	Flat surface	CFRP	Two	Surface condition
	B <sub>GM-G1-C2</sub>	SHGC	With one groove	CFRP	Two	
	B <sub>GM-G2-C2</sub>	SHGC	With two grooves	CFRP	Two	
	B <sub>GM-G1-S2</sub>	SHGC	With one groove	Steel	Two	
Group III	B <sub>GM-G1-G2</sub>	SHGC	With one groove	GFRP	Two	Reinforcement type
	B <sub>GM-G1-C2</sub>	SHGC	With one groove	CFRP	Two	
	B <sub>GM-G1-0</sub>	SHGC	With one groove	–	–	
Group IV	B <sub>GM-G1-C1</sub>	SHGC	With one groove	CFRP	One	Number of FRP layers
	B <sub>GM-G1-C2</sub>	SHGC	With one groove	CFRP	Two	
	B <sub>GM-G1-C3</sub>	SHGC	With one groove	CFRP	Three	

to the beam's depth. The length of the strengthened part was constant for the strengthened beams, which was 2000 mm. Before the strengthening applications, grooves were created in the soffit of nine beams. These grooves provide an additional contact area between the strengthening and the concrete substrate. A longitudinal groove with a depth of 25 mm and a width of 100 mm was created in eight beams. As for beam B<sub>GM-G2-C2</sub>, two grooves were created with a depth of 25 mm and a width of 50 mm. The created grooves represent the half of the concrete cover at the beam's soffit, following the procedure of Wakjira and Ebead (2018). For comparison, in one beam, the strengthening was applied in the form of an EB technique, thus, the surface of this beam (beam B<sub>GM-F-C2</sub>) was kept flat without grooves. The TRM strengthening system consists of a bonding mortar provided with textile reinforcement. In this work, the effect of three types of mortars was evaluated, namely; OM, SHCC and SHGC. Embedded into the strengthening mortar, either null, one, two or three layers of textile reinforcement were provided. The used textile reinforcement was either steel, GFRP or CFRP. Fig. 1 shows the arrangement of the textile layers inside the strengthening layer.

As presented in Table 1, the unstrengthened beam was designated by the letters “BC”. On the other hand, the strengthened beams were given the letter “B” followed by three symbols. The first refers to the type of mortar (OM=ordinary cementitious mortar; SC=SHCC; SG=SHGC). Where the second symbol refers to the surface condition (F=flat surface; G1=surface with one groove; G2=surface with two grooves). Finally, the last symbol refers to the type and number of the textile reinforcement layers (0, S, G and C=without reinforcement, Steel grid, GFRP textile and CFRP textile, respectively, where 1, 2 and 3=the number of the textile layers). For instance, the designation “B<sub>GM-G1-C2</sub>” refers to a test beam having a surface with a longitudinal groove and strengthened with a layer of strain-hardening geopolymer composites provided with two layers of the CFRP-textile.

## 2.2 Properties of Materials

### 2.2.1 Concrete

Table 2 lists the proportions of the used mixture. As shown in Table 2, the proportions of the mixture for every cubic meter were 350, 530, 1300 and 175 kg for ordinary Portland cement, sand (fine aggregate), crushed limestone (coarse

**Table 2** Mix proportions of the used concrete, ordinary mortar and SHCC for cubic meter (kg/m<sup>3</sup>).

Material	Cement	Sand	Coarse aggregate	Silica fume	Fibers (volumetric ratio)	Superplasticizers	Water	Water-to-binder ratio
Concrete	350	530	1300	–	–	–	175	0.50
OM	750	1350	–	–	–	20	225	0.30
SHCC	1342	157.9	–	237	16.20 (2.0%)	31.6	312.1	0.20



aggregate) and water, respectively. According to ASTM C39/C39M (2020), during the fabrication of the test specimens, three standard concrete cylinders were sampled for the compressive test. The cylinder had a diameter of 150 and a height of 300 mm. At the same time as the studied beams' testing, the compressive tests were performed on sampled cylinders. The mean compressive strength of the used concrete was 34.9 MPa.

### 2.2.2 Strengthening Mortars

Three different mortars were employed in the strengthening of the beams. Tables 2 and 3 show the mix proportions of these mortars. The proportions of ordinary cementitious mortar (OM) were selected following the recommendations of Baiee et al. (2017). The mix proportions were 1350 kg/m<sup>3</sup> of sand having a diameter of less than 0.2 mm, 750 kg/m<sup>3</sup> of ordinary Portland cement and 225 L/m<sup>3</sup> of water.

The proportions of the SHCC mixture are shown in Table 2. As recommended in several previous research (Ellithy et al., 2024; Li, 2003) cement type I and Silica fume were used as binder materials. The silica fume-to-cement ratio of was 18% (by weight). Fine sand with a nominal maximum size (N.M.S=0.2 mm) was utilized. The water-to-binder material ratio (W/B) was 20% (by weight). High-strength polypropylene (PP) fibers ( $V_f=2\%$ ) were used to improve the tension strength of the mortar. As presented in the manufacturer's datasheet, the fiber's aspect ratio, diameter and length were 480, 25  $\mu\text{m}$  and 12 mm, respectively.

In general, SHGC is composed of solid source materials alongside an activator solution that acts as the dissolving agent. As recommended by Shaikh et al. (2018), the mix proportions of the solid source materials and the activators (alkali source) used in the study are shown in Table 3. The solid source materials were the Fly Ash (FA) and Ground Granulated Blast Furnace Slag (GGBS). The activator solution consisted of sodium silicate and sodium hydroxide with a molarity of 16. The ratio of the sodium silicate to the sodium hydroxide ( $\text{Na}_2\text{SiO}_3/\text{NaOH}$ ) equals 2.5. To prepare the activator, the solution of the sodium hydroxide was prepared, after 24 h, the sodium silicate was added to this solution and then left for 3 h to cool down before the mixing process. In the mixing process, the fly ash, slag, sand and alkali activators were mixed for approximately 3 min. In addition, PP fibers with a volume fraction of 2% were added to the wet mixture.

During the strengthening application, samples from the used bonding mortars were prepared to obtain their mechanical characteristics. The uniaxial compressive test was carried out on six standard cylinders of 50 mm diameter and 100 mm height, as per JSCE (2008). The compressive strengths of the OM, SHCC and SHGC were 35.01, 55.81 and 48.20 MPa, respectively. Meanwhile, according to Shaikh et al. (2018) recommendations, the uniaxial tensile behaviour of the used mortars was assessed by testing six samples each. The dimensions of the specimens are shown in Fig. 2 (Shaikh et al., 2018). The samples had a total length of 500 mm and a cross-sectional area of  $20 \times 100 \text{ mm}^2$ . Two steel plates were fixed at the ends of the test sample to hold the test specimen. The overlap between the test sample and the steel plates was 100 mm. Two strain gauges (50 mm gauge length) were bonded in the middle of the sample to measure the tensile strain. The samples were tested in a displacement control loading manner under a strain rate of  $10^{-4}$  strain/second (Shaikh et al., 2018). Samples of the failure mode of the tested specimens are shown in Fig. 2b. As shown in the figures, the specimen of the OM demonstrated a localized cracking mode, whereas the strain-hardening mortars (SHCC and SHGC) developed multiple cracks before failure. Samples of the obtained stress–strain relationships are plotted in Fig. 2c. In addition, Table 4 summarizes the obtained results of the tested samples. The average ultimate tensile strengths for the tested OM, SHCC and SHGC specimens were 3.50, 6.62 and 7.21 MPa, respectively. The improved tensile strength of the SHGC material is owing to the replacement of the cement in SHCC with other admixtures to form the eco-friendly SHGC.

The bond strength between the substrate concrete and the strengthening material is one of the main important issues. Following ASTM C882 (1999), slant shear tests were carried out on three standard cylinders for each. The total height of the tested cylinders was 200 mm and the diameter was 100 mm. First, the bottom half of the cylinder was filled with the used concrete mixture. Before the application of the mortar, the concrete interface was cleaned using a rotary brush, and then, the mortar was cast over a water-saturated substrate. At the test date of the beam specimens, the slant test specimens were crushed under a compression test machine. The slant shear strength of the used mortars is summarized in Table 4. As shown in Table 4, the SHGC had the highest strength compared to the OM and SHCC. The mean strength of the OM, SHCC and SHGC were 4.47,

**Table 3** Mix proportions of the used SHGC for cubic meter (kg/m<sup>3</sup>).

Slag	Fly ash	Sand	Water	NaOH	$\text{Na}_2\text{SiO}_3$	Superplasticizers	Fibers (volumetric ratio)
400	600	150	100	100	250	10	16.20 (2.0%)

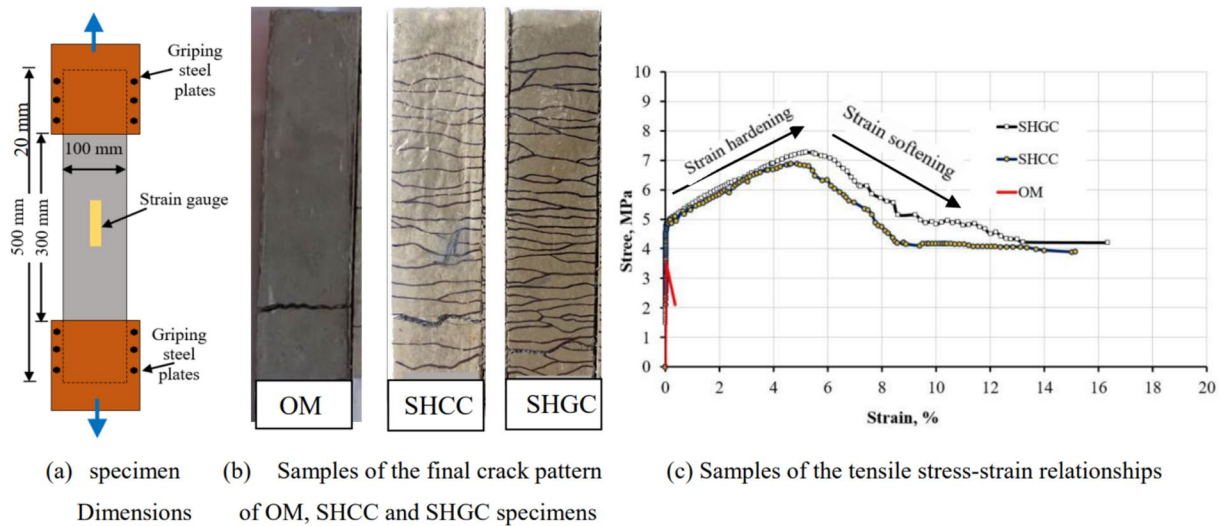


**Fig. 2** Details of the tensile test for the used mortars.

**Table 4** Summary of mortars' test results.

Mortar type	Compressive strength (MPa)	Tensile strength (MPa)		Slant shear strength (MPa)
		First cracking	Ultimate strength	
OM	35.01	3.50	3.50	4.47
SHCC	55.81	4.54	6.62	10.20
SHGC	48.20	5.15	7.21	14.60

10.20 and 14.60 MPa, respectively. These results reflect the higher bond strength of the SHGC than the other mortars.

### 2.2.3 Internal Steel Reinforcement

For the used types of steel bars, the uniaxial tensile test was mounted on three standard steel samples per

each. For the bars with a diameter of 10 mm, the yield strength ( $f_y$ ) and ultimate tensile strength ( $f_{ult}$ ) were 535 and 660 MPa, respectively. As for the bars with a diameter of 12 mm, the yield strength and ultimate tensile strength were 560 and 680 MPa, respectively.

### 2.2.4 Textile Reinforcement

In this investigation, three types of textile reinforcement were used; steel mesh, GFRB textile and CFRB textile. Fig. 3 shows samples of the used grid reinforcement. As obtained from the manufacturer's datasheet, the summary of the used textiles properties is presented in Table 5. The textiles were selected to achieve nearly the same tensile load capacity for every layer.

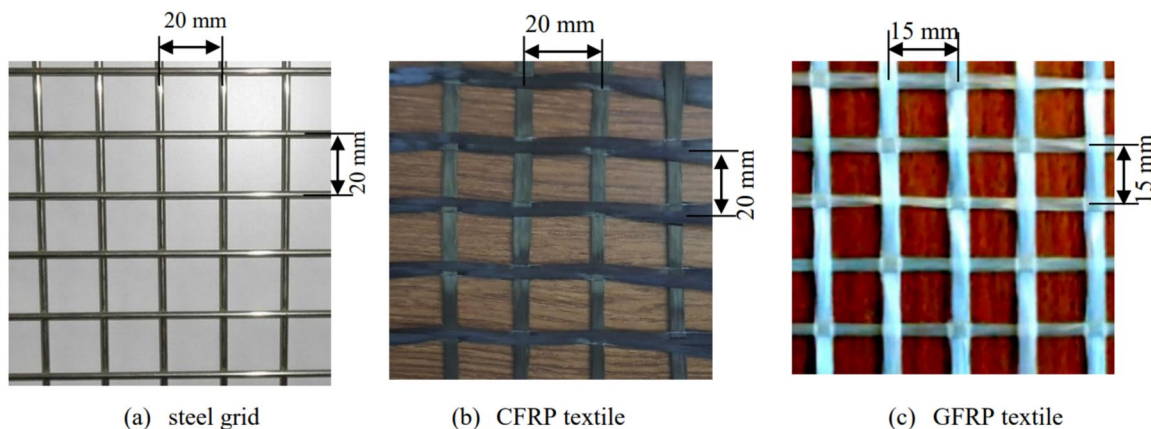


**Fig. 3** Samples of the used textiles.

### 2.3 Strengthening Application

Fig. 4 shows the steps of the strengthening application. At the age of 28 days after concrete casting, the strengthened beams were turned over (i.e., the bottom surface was upward). The grooves were created using a slitting machine based on the strengthening regime. Then the beam's substrate surface was roughened using a rotary brush and cleaned with an air compressor. A wooden formwork was fixed into both sides of the beams. After mixing the mortar, the first layer of the used mortar was cast on the strengthened area, and then the first layer of the textile was placed and carefully pressed into the mortar. Afterward, another layer of mortar was applied to cover the textiles. For the beams with more than one textile layer, the steps mentioned above were repeated. To avoid the misalignment of the textile fibers, guiding remakes were positioned at the side faces of the wooden shuttering. To improve the ultimate strain capacity of the used FRP textiles, the FRP textiles were impregnated with epoxy before the strengthening application (Nematollahi et al., 2014). After completion of the strengthening process, all the SHGC-strengthened beams were ambient cured at an average temperature of 32 °C for 28 days

before testing. The SHCC/OM strengthened beams were cured using wet clothes for 14 days and then left to dry before testing.

### 2.4 Test Setup and Instrumentations

Fig. 5 depicts the test setup and instrumentation. As presented in this figure, the tests were carried out through a four-point bending pattern. The beams were placed over a roller and a hinged supports. The load was applied over a rigid steel beam supported over two loading plates. The distance between the loading plates was 600 mm, and the effective span of the tested beam specimen was 2200 mm. A hydraulic jack with an ultimate capacity of 400 kN was used. Through the test, the developed deflections were measured using a series of linear variable transducers of 100 mm gauge length. Electrical strain gauges with a gauge length of 10 mm were used to measure the tensile strains in the longitudinal steel reinforcing bars and the textiles. During the fabrication stage of the beams, the location of the strain over the steel bar was first grinded and then cleaned using acetoin. Following, the strain gauge was glued on the bar and then protected using a plastic sheet covered with silicon. In addition,

**Table 5** Properties of the used textile reinforcement.

Type of reinforcement	No. of filament/ bundle	Diameter of filament (mm)	Area of one bundle (mm <sup>2</sup> )	Spacing of bundles (mm)	Area of fabric per unit mm <sup>2</sup> /mm width	Tensile strength (MPa)	Tensile modulus (GPa)
CFRP	12,000	0.007	0.461	20	0.023	4000	240
GFRP	19,500	0.008	0.980	15	0.065	1375	80
Steel mesh	1	3.0	7.06	20	0.353	240/350*	200

\* Yield/ultimate strength.



**Fig. 4** Images of different stages of strengthening application.



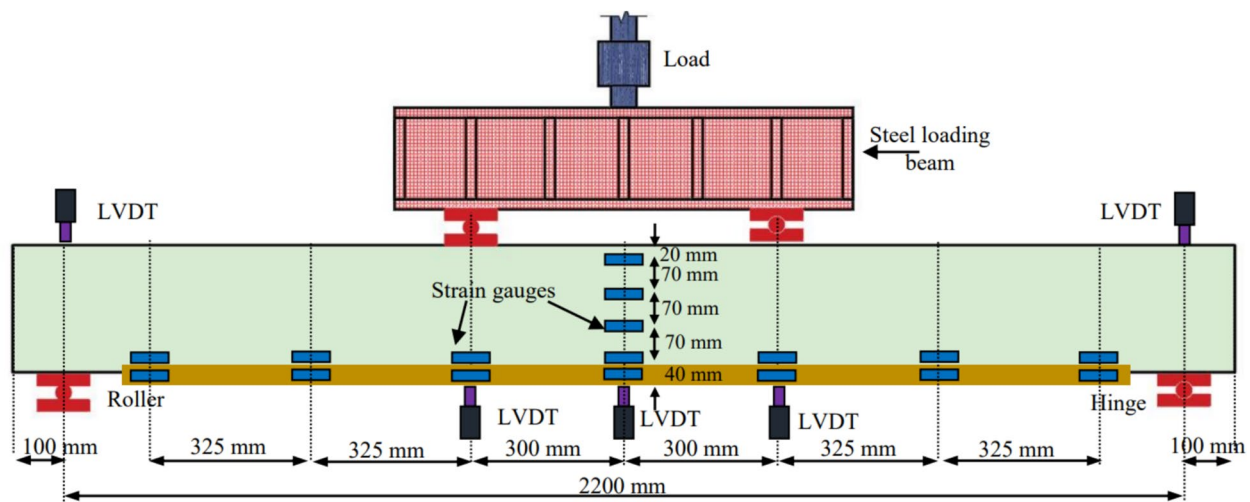


**Fig. 5** Test setup and instrumentation.

strain gauges with a length of 50 mm were bonded on the beams' surfaces to measure the concrete strains over the beam's depth and along the strengthened length. At different load intervals, a digital microscope with an accuracy of 0.01 mm was used to measure the maximum crack width. The values of the deflections and strains corresponding to each load increment were recorded using a data logger system.

### 3 Experimental Results

#### 3.1 Failure Mode

Figs. 6 and 7 show the final cracking pattern and failure modes of the studied beams. As shown in Fig. 7a, as expected based on design, the control beam exhibited flexural tension failure typical of under-reinforced sections. The beam failed due to the yielding of the internal tension steel bars followed by concrete crushing at the compression zone. For the strengthened beams, after the yielding of internal steel bars, the beams showed three different modes of failure. (1) For beam  $B_{OM-G1-C2}$ , as shown in Fig. 7b, the failure was a slippage of the FRP textile accompanied by intermediate crack (IC) debonding. (2) For beam  $B_{GM-F-C2}$ , as shown in Fig. 7c, the failure was governed by an intermediate crack debonding between the strengthening mortar and the concrete substrate at the constant moment zone. (3) For beams  $B_{CM-G1-C2}$ ,  $B_{GM-G1-C2}$ ,  $B_{GM-G2-C2}$ ,  $B_{GM-G1-S2}$ ,  $B_{GM-G1-G2}$ ,  $B_{GM-G1-O}$ ,  $B_{GM-G1-C1}$  and  $B_{GM-G1-C3}$ , the failure was a rupture of the used textile followed by concrete crushing. Fig. 7d shows a sample of the obtained mode of failure for beam  $B_{GM-G1-C2}$ . As shown in Fig. 7d, no sign of debonding was noticed between the strengthening layer and the concrete substrate. This is owing to the good bond of the

strain-hardening mortars, in addition, the NSEEB technique increased the contact area between the bonding mortar and the concrete substrate.

#### 3.2 Cracking and Ultimate Loads

Table 6 summarizes cracking and ultimate loads, showing a consistent increase in the ultimate loads for beams with SHGC strengthening. As shown in Table 6, the unstrengthened beam had the lowest results of cracking and ultimate loads of 17.2 and 63.5 kN, respectively. For beam  $B_{OM-G1-C2}$ , a slight enhancement in the cracking load was recorded. The cracking load was 18.3 kN (6% higher than that obtained by beam BC). Whereas, for the others (strengthened with SHGC/SHCC), the improvement in the cracking loads ranged between 19 and 28% of that achieved by the control beam. This improvement is owing to the enhanced cracking strength of the strain-hardening mortars. Regarding the ultimate loads, for group I, the use of textile-reinforced mortars increased the ultimate capacity. Beam  $B_{OM-G1-C2}$  (strengthened with OM) achieved a load capacity of 82.12 kN, which is 29% higher than that of the control beam (BC). Whereas, beams  $B_{CM-G1-C2}$  and  $B_{GM-G1-C2}$  achieved ultimate capacities of 97.31 and 102.18 kN, respectively. These values represent about 53 and 61%, respectively, higher than beam BC. The enhancement in the ultimate capacity, especially with the use of SHGC, resulted from the improved tension stiffening of strain-hardening composites.

The use of the NSEEB technique with beams  $B_{GM-G1-C2}$  (the substrate concrete with one groove) and  $B_{GM-G2-C2}$  (the substrate concrete with two grooves), increased the interfacial contact between the strengthening mortar



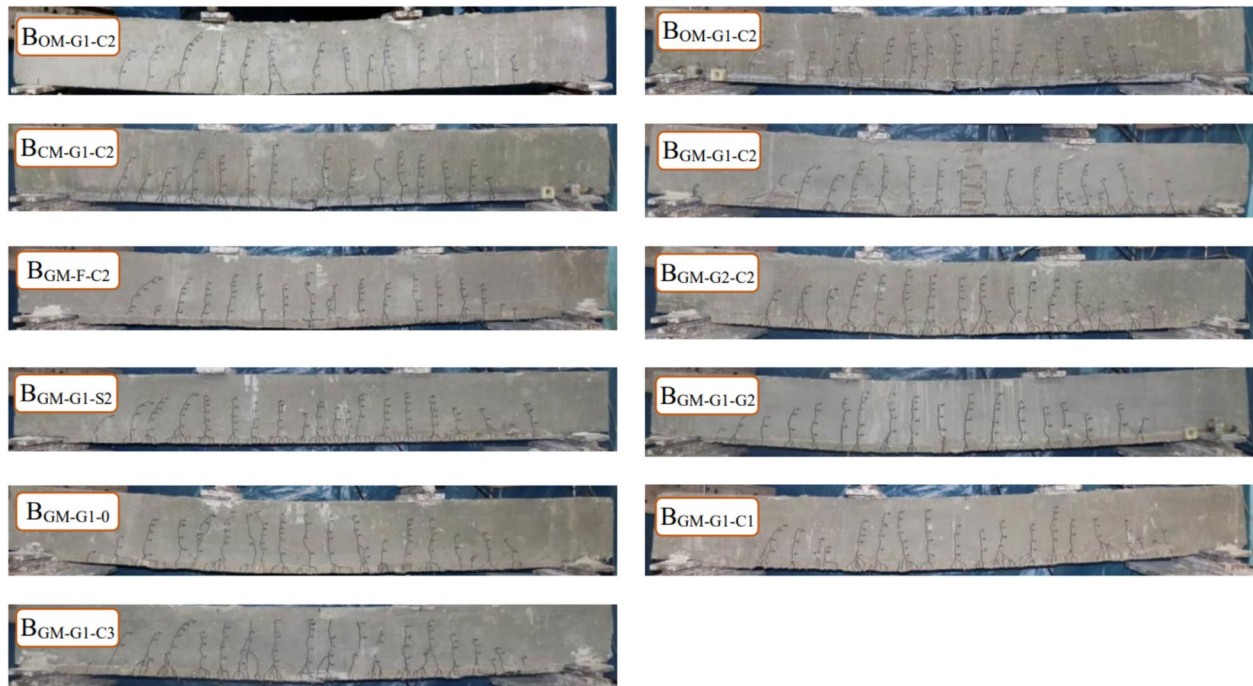


**Fig. 6** Final cracking patterns of the tested beams.

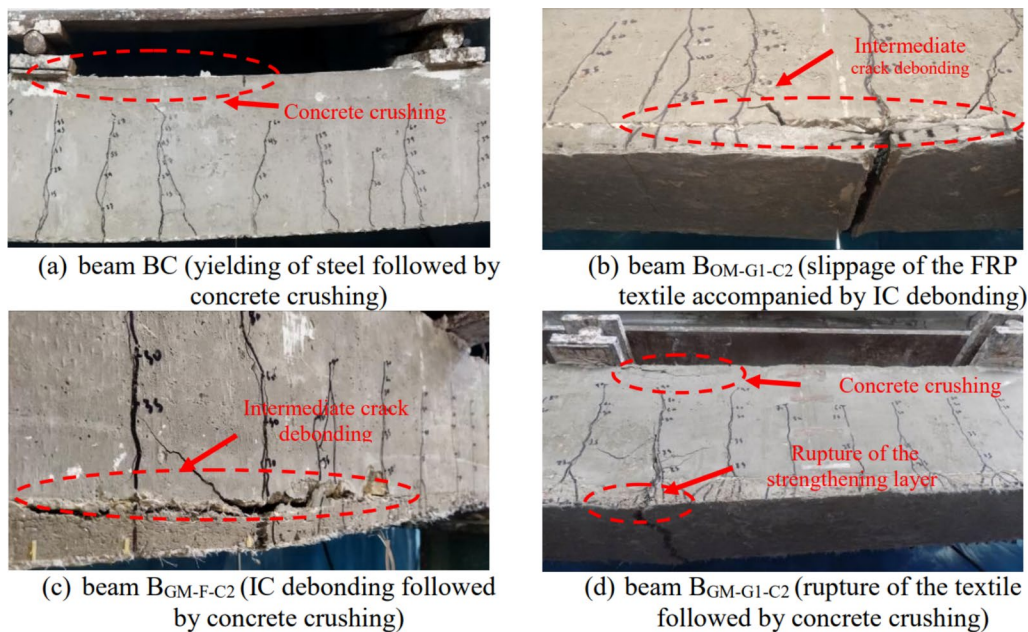


**Fig. 7** Failure modes of the tested beams.

and the substrate concrete. That prevented the debonding failure and increased the cross-sectional area of the added mortar. Accordingly, the ultimate loads of beams  $B_{GM-G1-C2}$  and  $B_{GM-G2-C2}$  were higher than beam  $B_{GM-F-C2}$  (with a flat surface). For beams  $B_{GM-G1-C2}$  and

$B_{GM-G2-C2}$ , the achieved loads were 20 and 21%, respectively, higher than that of beam  $B_{GM-F-C2}$  ( $P_u = 85.11$  kN).

Regarding group III, three types of textile reinforcement were used with nearly the same design tensile capacity. Thus, the beams showed a negligible variation

**Table 6** Summary of test results.

Groups	Beam	At first crack			At the yield of steel reinforcement			At ultimate load			$\mu$ (mm/mm)	E (kN.mm)
		P (kN)	P/P <sub>BC</sub>	$\Delta$ (mm)	P (kN)	P/P <sub>BC</sub>	$\Delta$ (mm)	P (kN)	P/P <sub>BC</sub>	$\Delta$ (mm)		
Control	BC	17.20	1.00	1.46	56.11	1.00	10.92	63.50	1.00	44.57	4.08	1722
Group I	B <sub>OM-G1-C2</sub>	18.30	1.06	1.15	69.10	1.23	10.91	82.12	1.29	18.10	1.65	514
	B <sub>CM-G1-C2</sub>	21.01	1.22	1.05	80.40	1.43	10.94	97.31	1.53	25.29	2.31	927
	B <sub>GM-G1-C2</sub>	21.52	1.25	1.04	81.70	1.46	11.15	102.18	1.61	28.23	2.53	940
Group II	B <sub>GM-F-C2</sub>	21.42	1.24	1.26	80.21	1.43	9.75	85.11	1.34	18.57	1.90	525
	B <sub>GM-G2-C2</sub>	21.77	1.26	1.08	81.85	1.46	10.95	103.13	1.62	28.28	2.58	955
Group III	B <sub>GM-G1-S2</sub>	22.10	1.28	0.93	93.28	1.66	10.31	103.23	1.63	40.75	3.95	1707
	B <sub>GM-G1-G2</sub>	21.01	1.22	0.98	70.71	1.26	10.81	101.25	1.59	31.92	2.95	897
Group IV	B <sub>GM-G1-0</sub>	20.40	1.19	1.18	66.94	1.19	10.59	73.90	1.16	19.52	1.84	595
	B <sub>GM-G1-C1</sub>	20.48	1.19	0.97	74.04	1.31	10.72	91.52	1.44	25.11	2.34	742
	B <sub>GM-G1-C3</sub>	21.61	1.26	1.01	85.11	1.52	10.17	106.31	1.67	29.59	2.91	1005

P = load;  $\Delta$  = deflection;  $\mu$  = ductility index; E = absorbed energy.

in the ultimate loads. The ultimate loads of beams B<sub>GM-G1-S2</sub> (the mortar provided with steel grid) and B<sub>GM-G1-G2</sub> (the mortar provided with GFRP textile) were 103.23 and 101.25 kN, respectively. These values represent 101% and 99% of that achieved by beam B<sub>GM-G1-C2</sub> (the mortar provided with CFRP textile).

As for group IV, as expected, the increase in textile layers provided in the SHGC layer increased the load capacity; however, this increase is not proportional to the increased ratio of textiles. For beams B<sub>GM-G1-C1</sub>, B<sub>GM-G1-C2</sub> and B<sub>GM-G1-C3</sub>, the strengthening layers were provided with one, two and three CFRP layers, respectively, the obtained loads were 24, 38 and 44%, higher than beam B<sub>GM-G1-0</sub> (the strengthening mortar without textile reinforcement).

### 3.3 Load–Deflection Behaviour

The load–deflection curves for the studied beams are shown in Fig. 8. As shown in Fig. 8, the control beam (BC) showed almost a linear response until the first cracking load. At cracking, a significant loss in the beam stiffness took place, thus after cracking; an increase in the rate of the developed deflection was noticed. With the increase in applied load, the yield of the internal steel bars took place, and then the beam demonstrated almost a plastic load–deflection behaviour until failure. At ultimate, the value of the recorded deflection was 44.57 mm. As for the strengthened beams, as shown in Fig. 8, in general, the effect of the strengthening was limited in the primarily uncracked stage of loading. Whereas, beyond cracking, the presence of the strengthening layer improved the post-cracking stiffness, which decreased the developed deflection compared to the control beam (BC). In addition, after the yielding of the internal steel

bars, the FRP–SHGC strengthening increased the post-yielding stiffness. Finally, at the post-peak stage, except for beam B<sub>GM-G1-S2</sub> (strengthened with steel-reinforced SHGC), the strengthened beams showed a sudden loss of the strengthening action. The loss of the strengthening action was quite abrupt due to the nature of FRP failure. After failure, it is noticed that, the FRP–SHGC strengthened beams exhibited residual flexural capacity close to that of the control beam (BC).

As shown in Fig. 8a, both the SHGC and SHCC mortars showed improved post-cracking stiffness than the ordinary mortar due to the effect of fiber bridging, which decreased the developed deflection of beams B<sub>CM-G1-C2</sub>, and B<sub>GM-G1-C2</sub> compared to beam B<sub>OM-G1-C2</sub>. For instance, at the service deflection (L/250), beams B<sub>CM-G1-C2</sub>, and B<sub>GM-G1-C2</sub> achieved loads of 8.8 and 9.0%, respectively, higher than beam B<sub>OM-G1-C2</sub>. In addition, using SHGC or SHCC increased the ultimate deflection compared to OM. The maximum deflection of beams B<sub>CM-G1-C2</sub>, and B<sub>GM-G1-C2</sub> were 25.29 and 28.23 mm, respectively. These values represent about 39 and 56% higher than B<sub>OM-G1-C2</sub> ( $\Delta_u = 18.1$  mm).

Regarding group II, as shown in Fig. 8b, the use of either the NSEEB or EB technique did not alter the pre-ultimate stages of loading. Whereas, at the ultimate, using the NSEEB technique prevented the debonding failure, and this increased the developed deflection. For beams B<sub>GM-G1-C2</sub> and B<sub>GM-G2-C2</sub> the ultimate deflections were 28.23 and 28.28 mm, respectively, these values are about 52% higher than beam B<sub>GM-F-C2</sub> ( $\Delta_u = 18.57$  mm).

For group III, as shown in Fig. 8c, using steel mesh inside the SHGC layer showed the best behaviour at the post-cracking stage. At the same load level, beam B<sub>GM-G1-S2</sub> showed higher stiffness and lower deflection

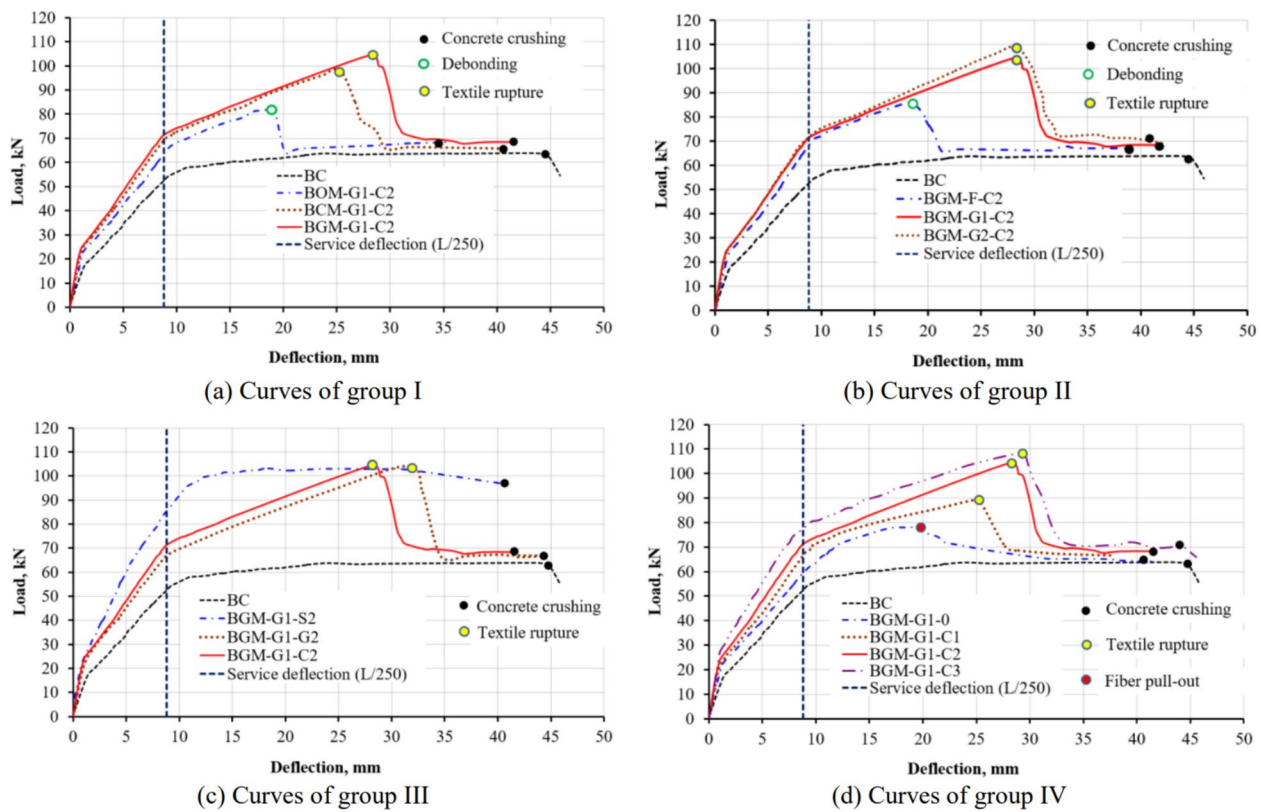


**Fig. 8** Load–deflection curves of the tested beams.

values compared to beams  $B_{GM-G1-G2}$  and  $B_{GM-G1-C2}$ . At the service deflection, beam  $B_{GM-G1-S2}$  reached a load capacity of 86.02 kN, which is 29 and 21% higher than those of beams  $B_{GM-G1-G2}$  and  $B_{GM-G1-C2}$ , respectively. This improvement in the beam stiffness ( $B_{GM-G1-S2}$ ) is a result of the higher modulus of elasticity of steel than the FRP-textiles. In addition, using steel mesh increased the post-ultimate ductility compared to the FRP-textiles, at ultimate, the maximum deflection of beam  $B_{GM-G1-S2}$  was 40.75 mm, which is 24 and 44% higher than those of beams  $B_{GM-G1-G2}$  and  $B_{GM-G1-C2}$ . This is attributed to the higher ductility of steel reinforcement compared to the FRP textiles, which have a limited tensile capacity.

As for group IV, as shown in Fig. 8d, increasing the number of FRP layers in the SHGC mortar increased the tension stiffness, which decreased the post-cracking deflection. For instance, at service deflection, the achieved loads of beams  $B_{GM-G1-C1}$ ,  $B_{GM-G1-C2}$  and  $B_{GM-G1-C3}$  were 67.48, 70.99 and 80.44 kN, respectively, which are 14, 20 and 36% higher than beam  $B_{GM-G1-0}$  (strengthened with unreinforced SHGC layer). Increasing the layers of the FRP textiles increased the ultimate deflection. For beams  $B_{GM-G1-0}$ ,  $B_{GM-G1-C1}$ ,  $B_{GM-G1-C2}$  and  $B_{GM-G1-C3}$ , the results of the ultimate deflection were 19.52, 25.11, 28.23 and 29.59 mm, respectively.

### 3.4 Ductility and Absorbed Energy

The deflection-based ductility index ( $\mu$ ) is defined as the ratio of the mid-span deflection at ultimate load ( $\Delta_u$ ) to that at yield load ( $\Delta_y$ ) (Hussein et al., 2012). Where the energy absorption index ( $E$ ) is defined as the accumulative area under the load–deflection curve from zero to the ultimate point (Hussein et al., 2012). The results of the ductility indices and absorbed energies are summarized in Table 6.

As shown in Table 6, the un-strengthened beam (BC) gave the height ductility index compared to the strengthened beams. The value of the ductility index for the control beam was 4.08. Where, for the strengthened beams, the application of the strengthening decreased the ductility index. For group I, the use of strain-hardening mortar showed better ductility performance than the ordinary mortar. For beams  $B_{CM-G1-C2}$ , and  $B_{GM-G1-C2}$ , the ductility indices were 2.31 and 2.53, respectively. These values are 40 and 53% higher than beam  $B_{OM-G1-C2}$  ( $\mu=1.65$ ). For group II, the NSEEB technique increased the contact area between the strengthening layer and the concrete substrate compared to the EB technique. That prevented the debonding failure and then increased the ultimate deflection and ductility. Thus, beams  $B_{GM-G1-C2}$  and  $B_{GM-G2-C2}$  achieved higher ductility indices than



$B_{GM-F-C2}$  (with a flat surface). The value of the ductility index for beam  $B_{GM-F-C2}$  was 1.90 (75% of beam  $B_{GM-G1-C2}$ ). For group III, using a steel grid inside the SHGC mortar increased the inelastic deformation before failure. Thus, beam  $B_{GM-G1-S2}$  showed the best ductility performance compared to the strengthened beams. The ductility index of beam  $B_{GM-G1-S2}$  was 3.95. This value is 33% and 56% higher than beams  $B_{GM-G1-G2}$  and  $B_{GM-G1-C2}$ , respectively. Regarding group IV, increasing the number of textile reinforcement layers inside the SHGC improved the ductility. The ductility indices for beams  $B_{GM-G1-C1}$ ,  $B_{GM-G1-C2}$ , and  $B_{GM-G1-C3}$  were 27, 37 and 58%, respectively, higher than that of beam  $B_{GM-G1-0}$ .

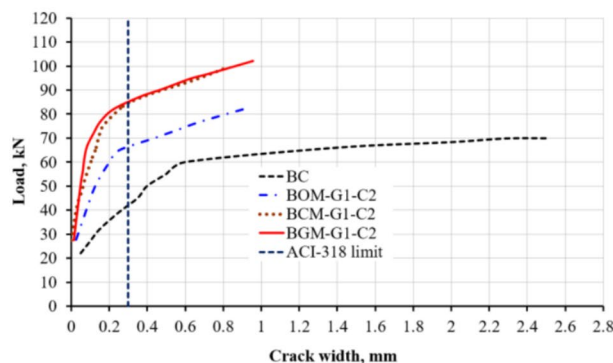
As presented in Table 6, the values of the absorbed energies showed almost a similar trend to the displacement-based indices. In general, the strengthening decreased the absorbed energy; however, the use of strain-hardening mortars showed higher absorbed energy compared to the ordinary mortar. The obtained energy for beams  $B_{CM-G1-C2}$  and  $B_{GM-G1-C2}$  were 927 and 940 kN.mm, respectively. These values are about 80 and 82%, respectively, higher than beam  $B_{OM-G1-C2}$ . In addition, beams  $B_{GM-G1-C2}$  and  $B_{GM-G2-C2}$  (strengthened with

the NSEEB technique) achieved energy values higher than beam  $B_{GM-F-C2}$  (strengthened with the EB technique). The obtained energy for beams  $B_{GM-G1-C2}$  and  $B_{GM-G2-C2}$  were 79 and 81%, respectively, higher than that of beam  $B_{GM-F-C2}$ . The use of the steel grid inside the SHGC showed the highest absorbed energy. The obtained energy for  $B_{GM-G1-S2}$  was 90 and 82% higher than those of beams  $B_{GM-G1-G2}$  and  $B_{GM-G1-C2}$ , respectively. Finally, for group IV, increasing the number of the FRP textile layers increased the absorbed energy. The absorbed energies of beams  $B_{GM-G1-C1}$ ,  $B_{GM-G1-C2}$  and  $B_{GM-G1-C3}$  were 25, 58 and 69%, higher than that of beam  $B_{GM-G1-0}$ , respectively.

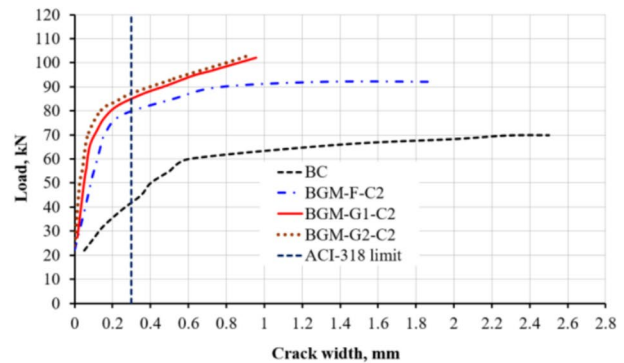
### 3.5 Crack Width Evolution

The load versus the measured maximum crack width is shown in Fig. 9. In addition, the service limit for the maximum crack width of ordinary exposed RC structures ( $W_{k,max}=0.30$  mm) is included in the figure for comparison ACI (2019).

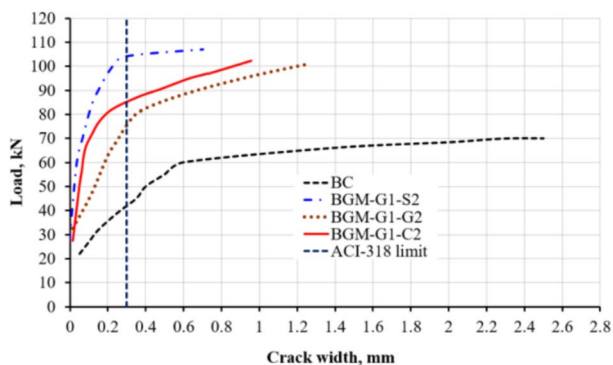
As shown in Fig. 9, for the control beam (BC), the crack width increased rapidly reaching a width of 0.3 mm (the service limit) at a load of 42 kN. Compared with the control beam, in general, the application of the strengthening



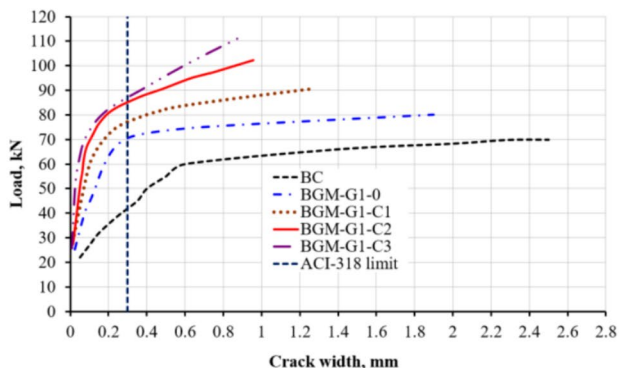
(a) Curves of group I.



(b) Curves of group II.



(c) Curves of group III.



(d) Curves of group IV.

**Fig. 9** Load crack width curves of the tested beams.



layer decreased the measured crack width at all stages of loading. Moreover, after the yielding of the steel bars, the use of FRP–SHGC strengthening prevented the rapid increase in the crack width. Comparing the load crack width of group I, the strain-hardening mortars showed lower crack width values than the ordinary mortar. This is owing to the tension-stiffening effect of strain hardening from fiber bridging. At a crack width of 0.3 mm, beam  $B_{OM-G1-C2}$  achieved a load of 68 kN, while beams  $B_{CM-G1-C2}$  and  $B_{GM-G1-C2}$  achieved 84 and 85 kN, respectively.

For group II, the NSEEB technique increased the contact surface between the concrete substrate and the strengthening layer. This improved the distribution of the tension cracks and then decreased the crack width of beams  $B_{GM-G1-C2}$  and  $B_{GM-G2-C2}$  (strengthened with the NSEEB technique), compared to beam  $B_{GM-F-C2}$ . At a crack width of 0.3 mm, beams  $B_{GM-G1-C2}$  and  $B_{GM-G2-C2}$  reached loads of 85 and 86 kN, respectively, which is 8 and 9% higher than that of beam  $B_{GM-F-C2}$  (at  $W_k = 0.30$  mm the achieved load = 79 kN).

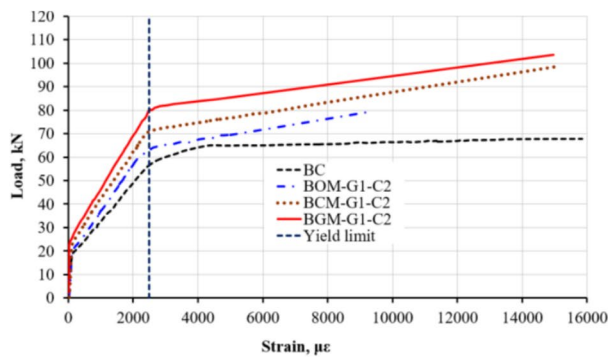
As for group III, as shown in Fig. 9c, the use of a steel grid inside the SHGC mortar decreased the maximum crack width than the FRP textiles. This is a result of the

higher elastic modulus of steel than the FRP. At a crack width of 0.3 mm, beam  $B_{GM-G1-S2}$  achieved a load of 105 kN, which is 23 and 40% higher than those of beams  $B_{GM-G1-C2}$  and  $B_{GM-G1-G2}$ , respectively.

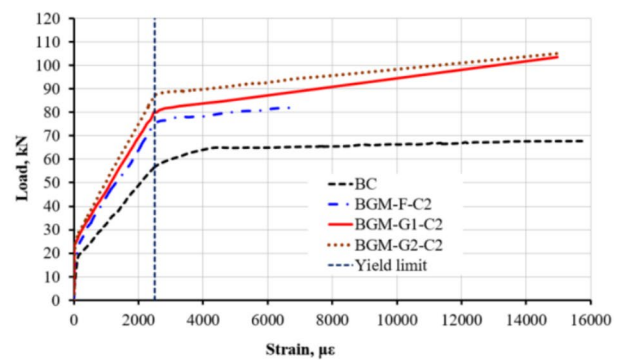
Regarding group IV, as expected, as shown in Fig. 9d, increasing the reinforcement ratio of the strengthening layer increased the tension stiffening and then decreased the crack width. For instance, at a crack width of 0.30 mm, beam  $B_{GM-G1-C3}$  (with three layers of CFRP inside the SHGC layer) reached a load of 91.50 kN, which represents 27% higher than that of beam  $B_{GM-G1-0}$  (with unreinforced SHGC layer).

### 3.6 Steel Strain

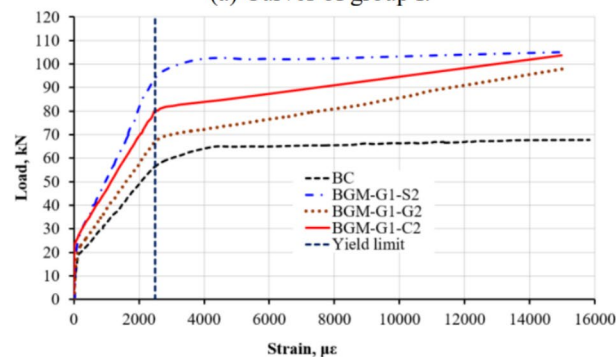
Fig. 10 shows the load versus the internal tension steel strains. As shown in Fig. 10, the strain curves are similar to the behavior described in load–displacement behaviour regarding the effects of mortar type, surface condition, the type of mortar reinforcement and the number of textile layers. Based on the carried out uniaxial tension tests, the yield strain of the steel bars was  $2500 \mu\epsilon$ . As shown in Fig. 10, at the same load, the control beam showed the highest strain value compared to the strengthened beams and reached the yield strain at



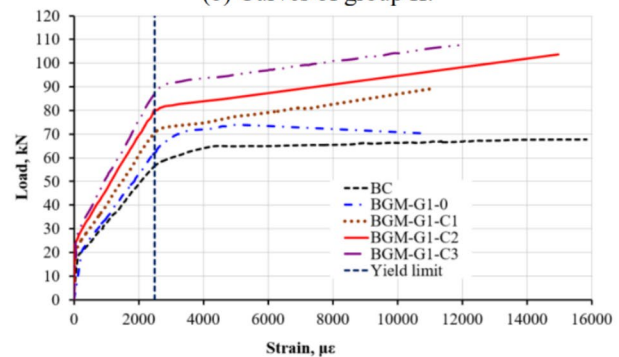
(a) Curves of group I.



(b) Curves of group II.



(c) Curves of group III.



(d) Curves of group IV.

**Fig. 10** Load strain curves of the tested beams.

a load of 56.11 kN. In addition, after the yielding of the steel reinforcement, the beam demonstrated a plastic behaviour until failure. On the other hand, the application of the strengthening layer reduced the steel strains, compared to the control specimen (BC). Moreover, after the yield load, the beams strengthened with FRP–SHGC layers demonstrated strain hardening, owing to the effect of the textile reinforcement. For group I, the use of strain-hardening mortar reduced the steel strain compared to the ordinary mortar and then increased the yielding load. For beams  $B_{CM-G1-C2}$  and  $B_{GM-G1-C2}$ , the yield loads were 80.40 and 81.70 kN, respectively. These loads represent 16 and 18%, respectively, higher than beam  $B_{OM-G1-C2}$  ( $P_y = 69.1$  kN). For group II, the use of either the NSEEB or EB technique showed an insignificant effect on the steel strain. The yield loads of beams  $B_{GM-F-C2}$  and  $B_{GM-G2-C2}$  were 80.21 and 81.85 kN, respectively. As for group III, the use of a steel grid inside the SHGC mortar decreased the strain compared to FRP textiles. The yield load of beam  $B_{GM-G1-S2}$  was 90.28 kN, which is 28 and 11% higher than those of beams  $B_{GM-G1-G2}$  and  $B_{GM-G1-C2}$ , respectively. For group III, as expected, the increase of textile layers inside the SHGC mortar decreased the steel strain. The yield loads of beams  $B_{GM-G1-0}$ ,  $B_{GM-G1-2}$  and  $B_{GM-G1-C3}$  were 66.94, 74.04 and 85.11 kN, respectively.

### 3.7 Strain Distribution

Fig. 11 depicts the strain distributions over the beam's height of the mid-span section. As shown in Fig. 11, the strains are plotted at different stages of loading corresponding to 0.30, 0.70 and 0.95 of the ultimate loads. For all beams, a linear behaviour of the strain distributions was observed at the pre-ultimate stages of loading. This indicates the applicability of bernoulli hypothesis. In addition, when the load increased, the neutral axis shifted up toward the compression zone. This is due to the growth of the concrete cracking at the tension side. Regarding the ultimate stage, beams  $B_{OM-G1-C2}$  (strengthened with OM applied in the form of the NSEEB technique) and  $B_{GM-F-C2}$  (strengthened with SHGC applied in the form of the EB technique) showed a sudden change in the strain distribution due to debonding failure. Whereas, the remaining strengthened beams showed almost linear strain distributions without any change in the strain slope. This reflects the complete bond between the applied strengthening and the concrete substrate.

Fig. 12 shows the strain distributions along the strengthening layer's length at different loading stages. In general, at the pre-ultimate stages, the strain profiles followed the bending moment shape indicating a complete bond between the applied strengthening and the concrete substrate. The maximum strain value is at the

mid-span and then the value decreases approaching the ends of the strengthening layer. At ultimate, except for beams  $B_{OM-G1-C2}$  and  $B_{GM-F-C2}$ , the strengthened beams demonstrated the same configuration of the pre-ultimate stages (the maximum strain value is at the mid-span). As for beams  $B_{OM-G1-C2}$  and  $B_{GM-F-C2}$ , the strain profile showed a flat plateau at the constant moment zone indicating no rupture in the textile layers, which confirms the obtained mode of failure that was intermediate crack debonding.

### 4 Prediction of Flexural Strength

During the experiments, the beams exhibited two distinguished modes of failure. The first was a rupture of the textile reinforcement followed by concrete crushing the compression zone. The second mode was a debonding failure between the strengthening layer and the concrete substrate. The analytical model of this investigation is limited to the beams that exhibited textile rupture at failure, thus strain compatibility could be applied. Fig. 13 shows the strains and stress diagrams for the strengthened beams. Based on the equilibrium of forces, the ultimate flexural moment could be obtained considering the following assumptions:

- As reflected by the test results, a perfect bond between the strengthening layer and the concrete substrate is assumed,
- The tensile capacity of strain hardening mortars was taken into consideration based on JSCE (2008) assumptions,
- The steel response is an elastic–plastic material under tension,
- The ultimate compressive strain ( $\epsilon_{cu}$ ) for concrete equals 0.003, as per ACI-318 (2019),
- The TRM has a linear behaviour up to failure and the maximum effective stress in the FRP ( $f_e$ ) can be calculated by the following equation:

$$f_e = E_f \epsilon_{fe} \quad (1)$$

$$\epsilon_{fe} = \epsilon_{cu} \left( \frac{d_f - c}{c} \right) \leq \epsilon_{fu} \quad (2)$$

where

$E_f$ =modulus of elasticity;  $\epsilon_{cu}$ =ultimate compressive strain of concrete;  $\epsilon_{fe}$ =effective tensile strain of FRP textile;  $\epsilon_{fu}$ =ultimate tensile strain of FRP textile;  $d_f$ =depth of textile reinforcement;  $c$ =depth of neutral axis.

Based on the above assumptions and the strains and stress distributions for the strengthened beams plotted in Fig. 13, the ultimate flexural moment is calculated using the following equation:

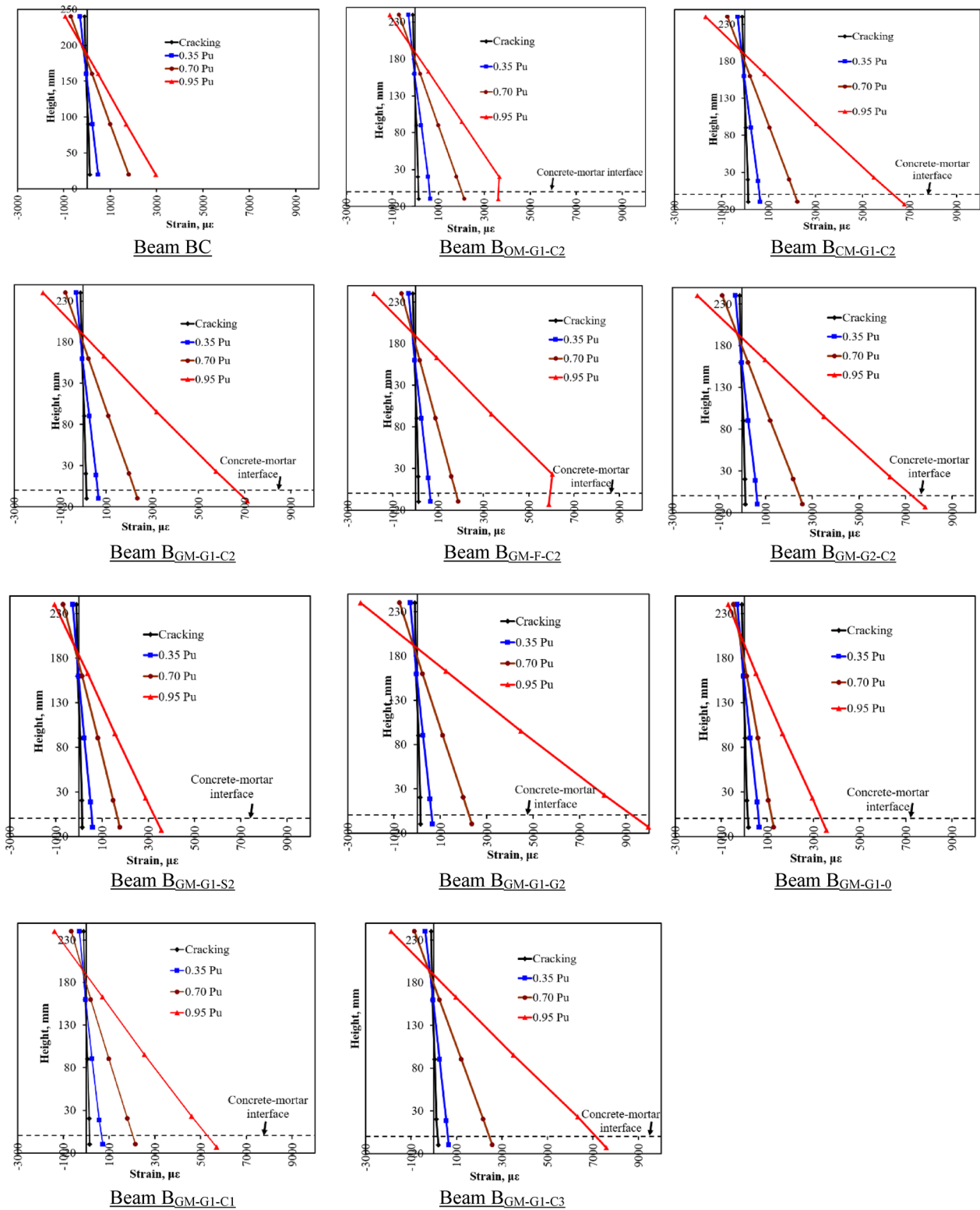


**Fig. 11** Sectional height versus concrete strain of the tested beams.

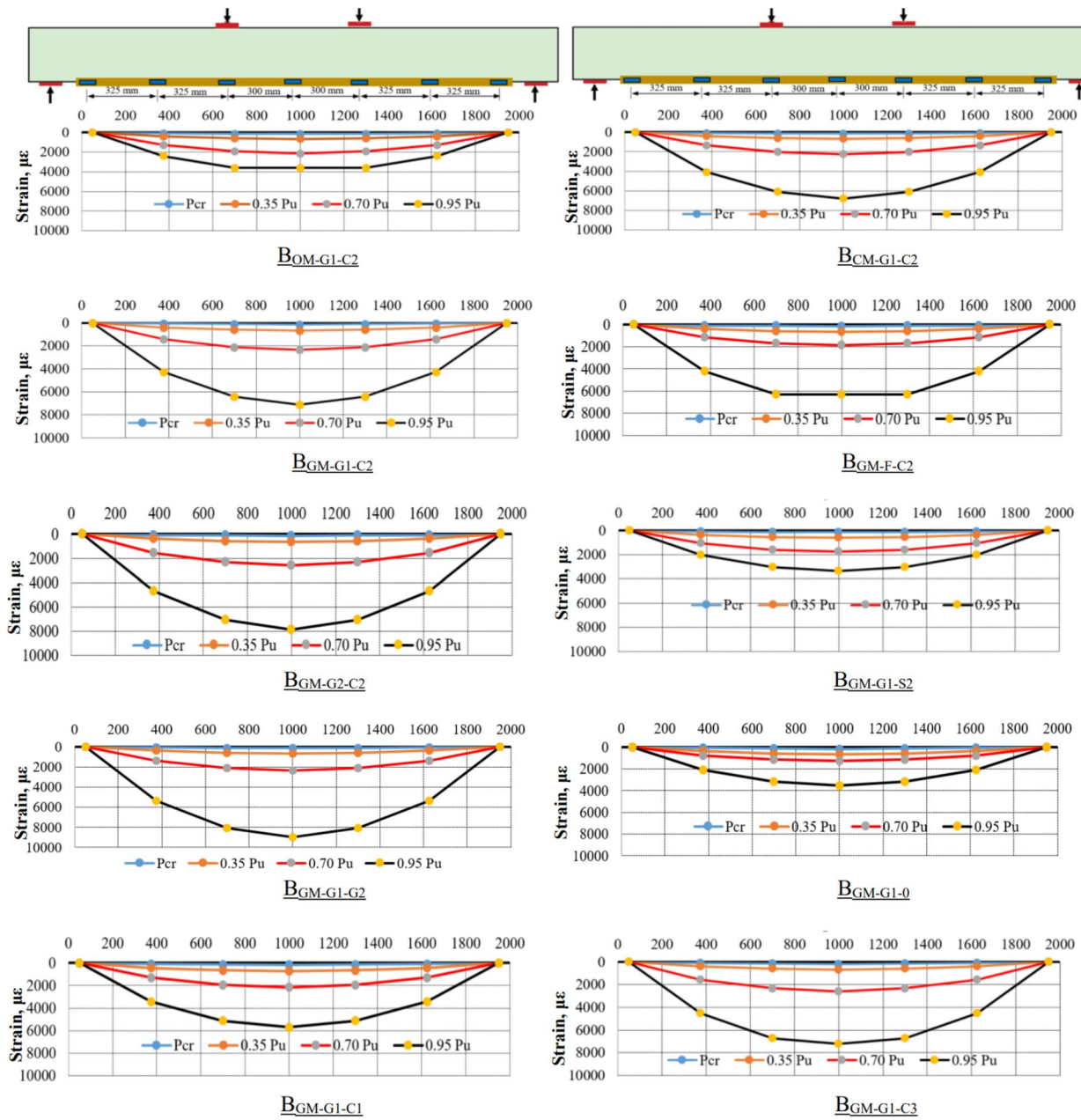


**Fig. 12** Strain distribution over the length of the strengthening layer.

$$M_u = T_s \left( d - \frac{\beta c}{2} \right) + T_f \left( d_f - \frac{\beta c}{2} \right) + T_{m1} \left( d_f - \frac{\beta c}{2} \right) + T_{m2} \left( d_c - \frac{t_c}{2} - \frac{\beta c}{2} \right) + C'_s (\beta c - d') \quad (3)$$

The internal forces ( $T_s$ ,  $T_f$ ,  $T_{m1}$ ,  $T_{m2}$  and  $C'_s$ ) can be calculated using Eqs. (7)–(10):

$$T_s = A_s f_s \quad (4)$$

$$T_f = N A_f b E_f \varepsilon_{fe} \quad (5)$$

$$T_{m1} = A_{m1} f_{ty} \quad (6)$$



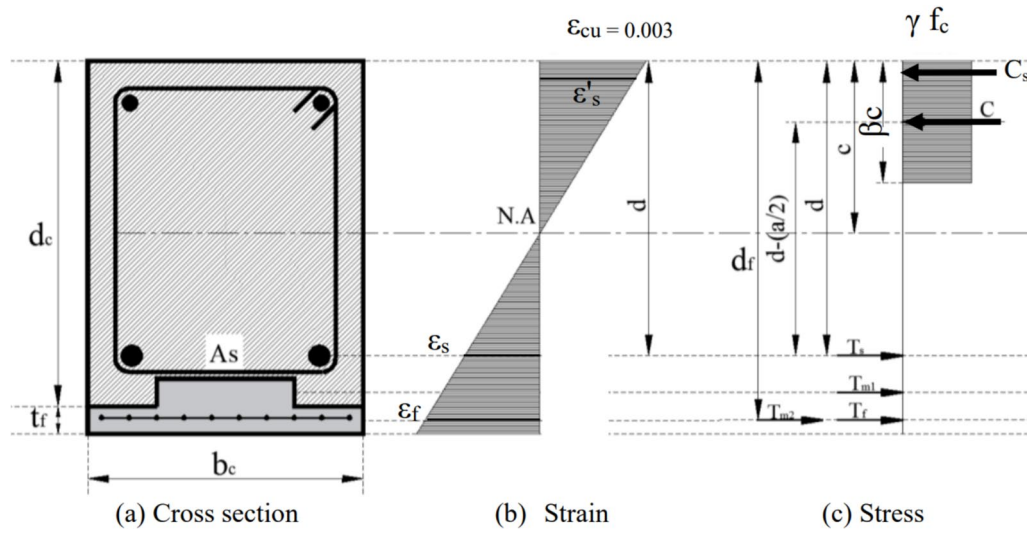


**Fig. 13** Strains and stresses diagrams for the strengthened beams.

$$T_{m2} = A_{m2}f_{ty} \quad (7)$$

$$C'_s = A'_s f'_s \quad (8)$$

According to the theory of strain compatibility, the stresses in the steel bars can be calculated using the following equations:

$$f_s = E_s \varepsilon_{cu} \left( \frac{d-c}{c} \right) \leq f_y \quad (9)$$

$$f'_s = E_s \varepsilon_{cu} \left( \frac{c-d'}{c} \right) \leq f_y \quad (10)$$

The depth of the neutral axis ( $c$ ) can be calculated based on the equilibrium of the forces from the following equation:

$$c = \frac{T_s + T_f + T_{m1} + T_{m2} - C'_s}{\alpha f'_c \beta b} \quad (11)$$

The concrete stress block factors  $\alpha$  and  $\beta$  are calculated as follows:

$$\beta = \frac{4\varepsilon'_c - \varepsilon_{cu}}{6\varepsilon'_c - 2\varepsilon_{cu}} \quad (12)$$

$$\alpha = \frac{3\varepsilon'_c \varepsilon_{cu} - \varepsilon_{cu}^2}{3\beta \varepsilon_c'^2} \quad (13)$$

The compressive strain of the unconfined concrete ( $\varepsilon'_c$ ) can be calculated using the following equation:

$$\varepsilon'_c = \frac{1.7f'_c}{E_c} \quad (14)$$

$$E_c = 4700\sqrt{f'_c} \quad (15)$$

where

$T_s$ ,  $T_f$  and  $T_m$  = the tensile forces of tension steel bars, the textile and the strain hardening mortar, respectively;  $C'_s$  = the compressive force carried by compression steel reinforcement;  $f'_c$  = the compressive strength of concrete;  $f_{ty}$  = the tensile yield strength of strain hardening mortars (First cracking strength according to JSCE (2008));  $f_s$  = the stress in steel reinforcement;  $f'_s$  = the stress of steel reinforcement at compression side;  $A_m$  = the cross section of strain hardening mortar;  $A_s$  = the cross-sectional area of tension steel reinforcement;  $t_c$  = section total thickness;  $b$  = width of the concrete beam;  $d$  = effective depth of concrete beam;  $d'$  = depth of compression steel;  $\alpha$  and  $\beta$  = The stress block factors.

The predicted results of the proposed model are listed in Table 7. As presented in Table 7, the predicted results of the ultimate moment capacity of the strengthened beams are close to the experimental results. The average of the experimental to the predicted flexural capacity ratio was 1.04 with a standard deviation of 0.056.

## 5 Conclusion

This research proposed a new composite system of FRP-SHGC as a strengthening system for RC beams. In this study varying parameters were studied; the type of the strengthening mortar (OM, SHCC and SHGC),

**Table 7** Experimental versus predicted results for ultimate moments.

Groups	Beam	$P_{u, \text{experimental}}$ (kN)	$M_{u, \text{experimental}}$ (kN.m)	$M_{u, \text{analytical}}$ (kN.m)	$P_{u, \text{experimental}}/P_{u, \text{analytical}}$
Control	BC	63.50	25.40	21.94	1.16
Group I	B <sub>OM-G1-C2</sub>	82.12	32.85	31.72	1.04
	B <sub>CM-G1-C2</sub>	97.31	38.92	37.54	1.04
	B <sub>GM-G1-C2</sub>	102.18	40.87	38.48	1.06
Group II	B <sub>GM-F-C2</sub>	85.11	34.04	36.23	0.93
	B <sub>GM-G2-C2</sub>	103.13	41.25	38.48	1.07
Group III	B <sub>GM-G1-S2</sub>	103.23	41.29	39.39	1.05
	B <sub>GM-G1-G2</sub>	101.25	40.50	38.99	1.04
Group IV	B <sub>GM-G1-0</sub>	73.90	29.56	28.51	1.04
	B <sub>GM-G1-C1</sub>	91.52	36.61	33.50	1.09
	B <sub>GM-G1-C3</sub>	106.31	42.52	43.47	0.97
				Mean	1.04
				SD	0.056
				COV	0.053

$P_{u, \text{experimental}}$  = experimental ultimate load;  $M_{u, \text{experimental}}$  = experimental ultimate moment =  $0.4 P_u$ ;  $M_{u, \text{analytical}}$  = predicted flexural moment.

the surface condition of the concrete substrate (flat and with grooves), and the reinforcement of the SHGC layer (type and ratio). The flexural behaviour of the studied beams was assessed through testing eleven reduced-scale RC beams. In addition, an analytical investigation was carried out to present a model for the flexural strength capacity of the FRP–SHGC-strengthened beams. Based on the current experimental and analytical results; the following conclusions are drawn:

- The use of the NSEEB technique in conjunction with SHGC precluded the occurrence of intermediate crack debonding failure and led to a rupture of the textile reinforcement, followed by concrete crushing.
- The composite use of FRP textile and strain-hardening mortar improved the cracking and ultimate loads. Compared to the unstrengthened beam, the cracking loads of the strengthened beams increased by values ranging between 6 and 26%, where ultimate load enhancements from 16 to 67% were achieved, varying by parameters, such as mortar and reinforcement types.
- Compared to the unstrengthened beam, the presence of the strengthening layer improved the post-cracking stiffness, which decreased the developed deflection. In addition, after the yielding of the internal steel reinforcement, the composite use of FRP textile and strain-hardening mortar developed a post-yielding stiffness.

- The use of the strengthening layer decreased the measured crack width at all stages of loading. Moreover, after the yielding of the internal steel reinforcement, the strengthening controlled the increase in the crack width.
- In general, compared to the unstrengthened beam, the strengthening reduced the ductility of the beams. As for the strengthened beams, the use of a steel grid inside the SHGC layer showed the best ductility performance, achieving a ductility index of 97% of the unstrengthened beam. Where the use of ordinary cementitious mortar showed the lowest ductility performance, achieving a ductility index of 40% of the unstrengthened beam.
- The proposed flexural strength prediction model gave a good prediction for the flexural capacity of the strengthened beams. The average value of the experimental/predicted results was 1.04 with a standard deviation of 0.056.

This research is a primary step to evaluate the response of RC beams strengthened in flexure with a composite layer of FRP–SHGC. This layer may be utilized for strengthening other structural concrete members, such as columns, slabs and beam–column connections. It should be noted that this study is limited to the studied scale of beams, the test parameters, and the properties of the used materials. In future work, the long-term and durability performances of RC beams strengthened with the FRP–SHGC layer should be studied. In addition, the efficacy of this technique under corrosion exposure needs to be evaluated.

#### Acknowledgements

The authors would like to acknowledge the staff of the RC laboratory of the faculty of engineering at Tanta University.

#### Author contributions

Mohamed Wasef: data curation, writing—original draft, and writing- review and editing. Ali Hassan: conceptualization, data curation, writing-original draft, and writing—review and editing. Nesreen M. Kassem: supervision and conceptualization. All authors read and approved the final manuscript.

#### Funding

Open access funding provided by The Science, Technology & Innovation Funding Authority (STDF) in cooperation with The Egyptian Knowledge Bank (EKB).

#### Availability of data and materials

All data generated or analyzed during this study are included in this published article.

#### Declarations

#### Competing interests

No competing interests exist in the submission of this manuscript, and manuscript is approved by all authors for publication. The authors declare that the work described was original research that has not been published previously and is not under consideration for publication elsewhere, in whole or in part.

Received: 3 September 2024 Accepted: 3 February 2025  
Published online: 19 May 2025

## References

- ACI. (2019). Building code requirements for structural concrete and commentary (ACI 318R-19). American Concrete Institute, Farmington Hills, MI, 519.
- Aljazeera, Z. R., Janke, M. A., & Myers, J. J. (2019). A novel and effective anchorage system for enhancing the flexural capacity of RC beams strengthened with FRCM composites. *Composite Structures*, 210, 20–28. <https://doi.org/10.1016/j.compstruc.2020.101873>
- Al Saffar, D. M., Tawfik, T. A., & Tayeh, B. A. (2020). Stability of glassy concrete under elevated temperatures. *European Journal of Environmental and Civil Engineering*, 26, 3157–3168. <https://doi.org/10.1080/19648189.2020.1783368>
- ASTM. (1999). Standard test method for bond strength of epoxy-resin systems used with concrete by Slant Shear C882-99. ASTM International, West Conshohocken, PA.
- ASTM. (2020). Standard test method for compressive strength of cylindrical concrete specimens C39/C39M-20. ASTM International, West Conshohocken, PA, [www.astm.org](http://www.astm.org).
- Baiee, A., Rafiq, I., & Lampropoulos, A. (2017). Innovative technique of textile reinforced mortar (TRM) for flexural strengthening of reinforced concrete (RC) beams. In Proceeding of the 2<sup>nd</sup> international conference on structural safety under fire and blast loading, London, UK, 11–12 September 2017; University of Brighton: London, UK.
- Bisby, L. A., Kodur, V. R., & Green, M. (2005). Fire endurance of fiber-reinforced polymer confined concrete. *ACI Structural*, 102, 883–891.
- Colajanni, P., Domenico, F. D., Recupero, A., & Spinella, N. (2014). Concrete columns confined with fibre reinforced cementitious mortars: Experimentation and modelling. *Construction and Building Materials*, 52, 375–384. <https://doi.org/10.1016/j.conbuildmat.2013.11.048>
- Dai, J., Ueda, T., & Sato, Y. (2005). Development of the nonlinear bond stress-slip model of fiber reinforced plastics sheet-concrete interfaces with a simple method. *Composites for Construction*, 9, 52–62. [https://doi.org/10.1061/\(ASCE\)1090-0268\(2005\)9:1\(52\)](https://doi.org/10.1061/(ASCE)1090-0268(2005)9:1(52))
- Duxson, P., Provis, J. L., Lukey, G. C., & van Deventer, J. S. J. (2007a). The role of inorganic polymer technology in the development of “green concrete.” *Cement and Concrete Research*, 37, 1590–1597. <https://doi.org/10.1016/j.cemconres.2007.08.018>
- Duxson, P., Fernández-Jiménez, A., Provis, J. L., Lukey, G. C., Palomo, A., & van Deventer, J. S. J. (2007b). Geopolymer technology: The current state of the art. *Materials Science*, 42, 2917–2933. <https://doi.org/10.1007/s10853-006-0637-z>
- Ellithy, M., Hassan, A., & El-Shafey, T. F. (2024). Flexural strengthening of RC beams using PGFRP bars embedded in strain-hardening cementitious composites (SHCC). *Engineering Structures*, 317, 118628. <https://doi.org/10.1016/j.engstruct.2024.118628>
- Elsanadedy, H. M., Almusallam, T. H., Alsayed, S. H., & Al-Salloum, Y. A. (2013). Flexural strengthening of RC beams using textile reinforced mortar—Experimental and numerical study. *Composite Structures*, 97, 40–55. <https://doi.org/10.1016/j.compstruc.2012.09.053>
- Faleschini, F., Zanini, M. A., Hofer, L., Toska, K., Domenico, D. D., & Pellegrino, C. (2020). Confinement of reinforced concrete columns with glass fiber reinforced cementitious matrix jackets. *Engineering Structures*, 218. <https://doi.org/10.1016/j.engstruct.2020.110847>
- Giese, A. C. H., Giese, D. N., Dutra, V. F. P., & Filho, L. C. P. D. S. (2021). Flexural behavior of reinforced concrete beams strengthened with textile reinforced mortar. *Building Engineering*, 33, 101873. <https://doi.org/10.1016/j.jobe.2020.101873>
- Gonzalez-Libreros, J. H., Sneed, L. H., D’Antino, T., & Pellegrino, C. (2017a). Behavior of RC beams strengthened in shear with FRP and FRCM composites. *Engineering Structures*, 150, 830–842. <https://doi.org/10.1016/j.engstruct.2017.07.084>
- Gonzalez-Libreros, J. H., Sabau, C., Sneed, L. H., Pellegrino, C., & Sas, G. (2017b). State of research on shear strengthening of RC beams with FRCM composites. *Construction and Building Materials*, 149, 444–458. <https://doi.org/10.1016/j.conbuildmat.2017.05.128>
- Hassan, A., Ellithy, M., & El-Shafey, T. F. (2022). Upgrading the shear strength of reinforced concrete corbels using strain hardening cementitious composites. *Engineering Structures*, 273, 115047. <https://doi.org/10.1016/j.engstruct.2022.115047>
- Hussein, M., Kunieda, M., & Nakamura, H. (2012). Strength and ductility of RC beams strengthened with steel-reinforced strain hardening cementitious composites. *Cement and Concrete Composites*, 34, 1061–1066. <https://doi.org/10.1016/j.cemconcomp.2012.06.004>
- Imjai, T., Setkit, M., Figueiredo, F. P., Garcia, R., Sae-Long, W., & Limkatanyu, S. (2022). Experimental and numerical investigation on low-strength RC beams strengthened with side or bottom near surface mounted FRP rods. *Structure and Infrastructure Engineering*, 19(11), 1600–1615. <https://doi.org/10.1080/15732479.2022.2045613>
- Imjai, T., Garcia, R., Kim, B., Hansapinyo, C., & Sukontasukkul, P. (2023). Serviceability behaviour of FRP-reinforced slatted slabs made of high-content recycled aggregate concrete. *Structures*, 51, 1071–1082. <https://doi.org/10.1016/j.jstruc.2023.03.075>
- Imjai, T., Guadagnini, M., Garcia, R., & Pilakoutas, K. (2016). A practical method for determining shear crack induced deformation in FRP RC beams. *Engineering Structures*, 126, 353–364. <https://doi.org/10.1016/j.engstruct.2016.08.007>
- JSCE. (2008). Recommendations for design and construction of high performance fiber reinforced cement composite with multiple fine cracks (HPFRCC). *Concrete Engineering*, 82.
- Kadhim, M. M. A., Jawdhari, A., Adheem, A. H., & Fam, A. (2022). Analysis and design of two-way slabs strengthened in flexure with FRCM. *Engineering Structures*, 256. <https://doi.org/10.1016/j.engstruct.2022.113983>
- Kong, D. L. Y., & Sanjayan, J. G. (2010). Effect of elevated temperatures on geopolymer paste, mortar and concrete. *Cement and Concrete Research*, 40(2), 334–339. <https://doi.org/10.1016/j.cemconres.2009.10.017>
- Koutas, L. N., & Papakonstantinou, C. G. (2021). Flexural strengthening of RC beams with textile-reinforced mortar composites focusing on the influence of the mortar type. *Engineering Structures*, 246, 113060. <https://doi.org/10.1016/j.engstruct.2021.113060>
- Kunieda, M., & Rokugo, K. (2006). Recent progress on HPFRCC in Japan—required performance and applications. *Advanced Concrete Technologies*, 4, 19–33. <https://doi.org/10.3151/jact.4.19>
- Lee, B. Y., Cho, C. G., Lim, H. J., Song, J. K., Yang, K. H., & Li, V. C. (2012). Strain hardening fibre reinforced alkali-activated mortar—A feasibility study. *Construction and Building Materials*, 37, 15–20. <https://doi.org/10.1016/j.conbuildmat.2012.06.007>
- Li, V. C. (1993). From micromechanics to structural engineering—the design of cementitious composites for civil engineering applications. *JSCE Journal of Structural Mechanics and Earthquake Engineering*, 10(2), 37–48. <http://hdl.handle.net/2027.42/84735>
- Li, V. C. (1998). Engineered cementitious composites for structural applications. *Materials in Civil Engineering*, 10(2), 66–79. [https://doi.org/10.1061/\(ASCE\)0899-1561\(1998\)10:2\(66\)](https://doi.org/10.1061/(ASCE)0899-1561(1998)10:2(66))
- Li, V. C. (2003). Engineered cementitious composites (ECC)—A review of the material and its applications. *Advanced Concrete Technologies*, 1(3), 215–230. <https://doi.org/10.3151/jact.1.215>
- Li, V. C., Wang, S., & Wu, C. (2001). Tensile strain-hardening behavior of polyvinyl alcohol engineered cementitious composite (PVA-ECC). *ACI Materials*, 98, 483–492. <https://doi.org/10.14359/10851>
- Li, Z., Ding, Z., & Zhang, Y. (2004). Development of sustainable cementitious materials. Paper presented at the proceedings of the international workshop on sustainable development and concrete technology.
- Liu, H., Zhang, Q., Gu, C., Su, H., & Li, V. (2017). Influence of microcrack self-healing behavior on the permeability of engineered cementitious composites. *Cement and Concrete Research*, 82, 14–22. <https://doi.org/10.1016/j.cemconcomp.2017.04.004>
- Lu, X. Z., Teng, J. G., Ye, L. P., & Jiang, J. J. (2005). Bond-slip models for FRP sheets/plates bonded to concrete. *Engineering Structures*, 27, 920–937. <https://doi.org/10.1016/j.engstruct.2005.01.014>
- Napoli, A., & Realfonzo, R. (2020). Compressive strength of concrete confined with fabric reinforced cementitious matrix (FRCM): Analytical models. *Composites Part C: Open Access*, 2, 100032. <https://doi.org/10.1016/j.jcomc.2020.100032>
- Nematollahi, B., Sanjayan, J. G., & Shaikh, F. U. A. (2014). Comparative deflection hardening behavior of fibre reinforced fly ash based geopolymer composites. *Construction and Building Materials*, 70, 54–64. <https://doi.org/10.1016/j.conbuildmat.2014.07.085>

- Nematollahi, B., Sanjayan, J. G., & Shaikh, F. U. A. (2015). Tensile strain hardening behavior of PVA fiber reinforced engineered geopolymer composite (PVA-EGC). *Materials in Civil Engineering*, 27(10). [https://doi.org/10.1061/\(ASCE\)MT.943-5533.0001242](https://doi.org/10.1061/(ASCE)MT.943-5533.0001242)
- Pan, B., Liu, F., Zhuge, Y., Zeng, J. J., & Liao, J. (2022). ECCs/UHPFRCs with and without FRP reinforcement for structural strengthening/repairing: A state-of-the-art review. *Construction and Building Materials*, 316, 125824. <https://doi.org/10.1016/j.conbuildmat.2021.125824>
- Peng, K. D., Huang, B. T., Xu, L. Y., Hu, R. L., & Dai, J. G. (2022). Flexural strengthening of reinforced concrete beams using geopolymer-bonded small-diameter CFRP bars. *Engineering Structures*, 256, 113992. <https://doi.org/10.1016/j.engstruct.2022.113992>
- Razak, S. N. A., Shafiq, N., Guillaumat, L., Wahab, M. M. A., Farhan, S. A., Husna, N., & Ismail, F. I. (2021). Fire performance of fly ash-based geopolymer concrete: Effect of burning temperature. *IOP Conference Series: Earth and Environmental Science*, 945.
- Sagoe-Crentsil, K., Brown, T., & Taylor, A. (2013). Drying shrinkage and creep performance of geopolymer concrete sustain. *Sustainable Cement-Based Materials*, 2, 35–42. <https://doi.org/10.1080/21650373.2013.764963>
- Sahmaran, M., Anil, Ö., Lachemi, M., Yildirim, G., Ashour, A., & Acađ F. (2015). Effect of corrosion on shear behavior of reinforced engineered cementitious composite beams. *ACI Structural*, 112, 771–782. <https://doi.org/10.14359/51687749>
- Shaikh, F. U. A. (2013). Deflection hardening behaviour of short fibre reinforced fly ash based geo-polymer composites. *Materials & Design*, 50, 674–682. <https://doi.org/10.1016/j.conbuildmat.2017.12.175>
- Shaikh, F. U. A., Fairchild, A., & Zammam, R. (2018). Comparative strain and deflection hardening behaviour of polyethylene fibre reinforced ambient air and heat cured geopolymer composites. *Construction and Building Materials*, 163, 890–900. <https://doi.org/10.1016/j.conbuildmat.2017.12.175>
- Shen, X., Chen, W., Li, B., Hancock, C. M., & Xu, Y. (2021). Flexural strengthening of reinforced concrete beams using fabric reinforced alkali-activated slag matrix. *Building Engineering*, 33, 101865. <https://doi.org/10.1016/j.jobe.2020.101865>
- Tetta, Z. C., Triantafillou, T. C., & Bournas, D. A. (2018). On the design of shear-strengthened RC members through the use of textile reinforced mortar overlays. *Composites Part B: Engineering*, 147, 178–196. <https://doi.org/10.1016/j.compositesb.2018.04.008>
- Wakjira, T. G., & Ebead, U. (2018). Hybrid NSE/EB technique for shear strengthening of reinforced concrete beams using FRCM: Experimental study. *Construction and Building Materials*, 164, 164–177. <https://doi.org/10.1016/j.conbuildmat.2017.12.224>
- Wakjira, T. G., & Ebead, U. (2019). A shear design model for RC beams strengthened with fabric reinforced cementitious matrix. *Engineering Structures*, 200, 109698. <https://doi.org/10.1016/j.engstruct.2019.109698>
- Wei, H., Li, Z. Q., Gao, W. Y., Zheng, P. D., & Guo, Z. X. (2020). Flexural behavior of RC beams strengthened with BFRP bars-reinforced ECC matrix. *Composite Structures*, 241, 112092. <https://doi.org/10.1016/j.compstruct.2020.112092>
- Yang, X., Gao, W. Y., Dai, J. G., Lu, Z. D., & Yu, K. Q. (2018). Flexural strengthening of RC beams with CFRP grid-reinforced ECC matrix. *Composite Structures*, 189, 9–26. <https://doi.org/10.1016/j.compstruct.2018.01.048>
- Ye, Y. Y., Smith, S. T., Zeng, J. J., Zhuge, Y., & Quach, W. M. (2021). Novel ultra-highperformance concrete composite plates reinforced with FRP grid: Development and mechanical behaviour. *Composite Structures*, 269, 114033. <https://doi.org/10.1016/j.compstruct.2021.114033>
- Zheng, Y. Z., Wang, W. W., Mosalam, K. M., & Zhu, Z. F. (2018). Mechanical behavior of ultrahigh toughness cementitious composite strengthened with fiber reinforced polymer grid. *Composite Structures*, 184, 1–10. <https://doi.org/10.1016/j.compstruct.2017.09.073>

**Ali Hassan** Associate Professor, Structural Engineering Department, Faculty of Engineering, Tanta University, Tanta, Egypt.

**Nesreen M Kassem** Professor, Structural Engineering Department, Faculty of Engineering, Tanta University, Tanta, Egypt.

## Publisher's Note

Springer Nature remains neutral with regard to jurisdictional claims in published maps and institutional affiliations.

**Mohamed Wasef** MSc candidate, Structural Engineering Department, Faculty of Engineering, Tanta University, Tanta, Egypt.